Mine Water Environ (2012) 31:3–15
DOI 10.1007/s10230-011-0166-0

TECHNICAL ARTICLE

Physical, Hydrologic, and Aqueous Chemical Characterization of the Ore Knob Tailings Pile (Ashe County, North Carolina, USA)

Mehrnoosh Behrooz · Robert C. Borden

Received: 24 June 2011 / Accepted: 1 November 2011 / Published online: 22 November 2011

Abstract Oxidation of pyrrhotite and related sulfide minerals in the vadose zone of the Ore Knob Mine tailings pile generates dissolved Fe^{+2}, SO_4^{-2}, and acidity, which are rapidly transported through the pile by infiltrating surface water. Significant spatial variations in the physical and hydraulic characteristics of the tailings cause large variations in air-filled porosity and effective oxygen diffusion into the pile. Tailings in the upstream areas are more fine-grained, with less air-filled porosity and oxygen diffusivity. The original tailings in the downstream areas are more coarse-grained, with less water retention and greater oxygen diffusivity. However, weathering processes have increased the fine-grained fraction in the oxidized zone and hardpan layer, increasing water retention and lowering oxygen diffusivity. The thickness of the downstream oxidized zone combined with increased water retention due to weathering may have significantly reduced acid generation in these areas.

Keywords Acid mine drainage · Hydrology · Ore Knob Mine · Particle size

Electronic supplementary material The online version of this article (doi:10.1007/s10230-011-0166-0) contains supplementary material, which is available to authorized users.

M. Behrooz (✉) · R. C. Borden
North Carolina State University,
Campus Box 7908, Raleigh, NC 27695, USA
e-mail: smbehroo@ncsu.edu

R. C. Borden
e-mail: rcborden@ncsu.edu

Introduction

Exposure of sulfide minerals to a moist, oxidizing environment often produces acid mine drainage (AMD) (Nordstrom and Alpers 1999; Singer and Stumm 1970) contaminants, including Al, As, Cd, Cu, Mn, Ni, Pb, and Zn (Parker and Robertson 1999). AMD may be released from a variety of sources including the mine itself, spoil mounds, and mineral tailings, severely impacting surface and groundwater resources. The US Environmental Protection Agency (USEPA 2004) identified 156 hardrock mining sites with total cleanup costs up to $24 billion, including 19 National Priorities List sites with potential remediation costs of over $50 million each.

Sulfide oxidation and acidity generation in tailings piles is often controlled by oxygen availability. In the saturated zone, oxygen transport is low since the oxygen diffusion rate in water is four orders of magnitude less than in air (Weast 1976). In the vadose zone, oxygen is primarily supplied by diffusion and advection through gas-filled pores (Jaynes et al. 1984; Nicholson et al. 1989; Pantelis and Ritchie 1991; Yanful et al. 1993). Since AMD generating reactions occur on the surface of sulfide minerals (Singer and Stumm 1970), mining processes that generate fine particles can increase the surface area exposed to oxygen and water, potentially increasing acid generation. However, fine-grained sediments also retain more water, reducing the gas-filled porosity and acid generation rates (Lottermoser 2007).

Near the tailings pile surface, the reduced sulfide content due to previous weathering of sulfide minerals exposes less reactive surfaces to oxygen, reducing acid generation. The thickness of this surface-oxidized zone will gradually increase over time, slowing oxygen diffusion into the pile (Gunsinger et al. 2006). However, rapid water infiltration

can potentially leach weathering products, exposing unoxidized mineral surfaces, and thus increasing oxidation rates (Gunsinger et al. 2006). In some cases, hardpans may develop as secondary minerals precipitate during infiltration through tailings (Blowes et al. 1991; Boorman and Watson 1976; McGregor et al. 1998; McSweeney and Madison 1988; Tasse et al. 1997). When the hardpan has smaller pores than the surrounding material, water may be retained, reducing the gas filled porosity, oxygen diffusion, and oxygen contact with sulfide minerals (Blowes et al. 1991; Gilbert et al. 2003; Johnson et al. 2000).

Acidity generation in tailings may also be influenced by mineralogy, moisture content, microbial activity, and temperature. The relative resistance of different minerals to oxidation varies due to differences in crystal structure and iron content (Schmiermund 2000). Generally, sulfide minerals containing large amounts of iron (e.g. pyrite, marcasite, and pyrrhotite) produce much more acidity than minerals lacking iron (e.g. sphalerite, galena, covellite; Lottermoser 2007; Plumlee 1999). Water serves as both the reaction medium and as an important reactant (Evangelou and Zhang 1995; Rose and Cravotta 1998). In arid environments, oxidation rates may be 2–3 times lower than rates in humidity cells due to reduced moisture content and larger particle size (Fennemore et al. 1998). Sulfur- and iron-oxidizing bacteria can catalyze the kinetic reaction of pyrite oxidation and increase the oxidation rate 30–300 fold (Nordstrom and Alpers 1999). Abiotic and biotic oxidation rates are temperature dependent and slow at the low temperatures associated with some mine sites (Escobar et al. 2009).

The Ore Knob Mine and Tailings Pile

Ore Knob, near Jefferson (Ashe County), North Carolina, is the location of a massive fissure-type sulfide deposit. The steeply dipping vein varies from 2.4 to 5.5 m thick and extends over 1,220 m along the contact between the Carolina gneiss and the adjoining muscovite—biotite schist (Rankin and Stuckey 1943). Pyrrhotite, pyrite, chalcopyrite, quartz, biotite, and amphiboles are the principal minerals in the vein (Kinkel 1967; Rankin and Stuckey 1943). From 1957 to 1962, Appalachian Sulphides, Inc., operated a mine and processing facility at the site, extracting copper, gold, and silver using a froth flotation and cyanide leaching process (Kinkel 1967; Rankin and Stuckey 1943). Most waste tailings were pumped to an impoundment located on Ore Knob Branch. A drop-inlet and 61-cm (24-inch) reinforced concrete pipe (RCP) were installed to provide drainage from the upstream end of the impoundment, through the dam, discharging into Ore Knob Branch. Over time, the embankment forming the dam was progressively raised to provide additional storage for the accumulated tailings, forming a 9 ha tailings pile with a maximum tailings depth of 21 m at the center of the embankment face. The surface elevation near the embankment face is approximately 6 m higher than near the drop-inlet, causing water to pool in this area, forming a small pond—wetland. The drop-inlet is located about 490 m from the face of the tailings. However, the outlet of the pipe has been covered by tailings, probably as a result of slope failure on the tailings embankment face.

Behrooz (2012) provides a detailed mineralogic and geochemical characterization of these tailings based on X-ray diffraction (XRD), scanning electron microscope with energy dispersive X-ray spectroscopy (SEM/EDS), and acid extraction measurements. Briefly, the tailings throughout the pile contain pyrrhotite, troilite, mackinawite, pyrite, quartz, and aluminosilicate minerals. SEM/EDS analyses indicate tailings collected below the water table have an atomic fraction of 18–22% Si, 10–15% Fe, 8–12% S, 2.8–6.6% Al, 2.2–2.7% Ca, 1.6–2.2% K, 0.7–2.9% Mg, 0.8–1.8% Na, and 0–0.2% Mn. Extraction of the sediment with HCl/HNO_3 and H_2O_2 following EPA method 3050 B and analysis by ICP-AES indicate that the tailings also contain 1.4–2.9 mg/g Zn and 0.8–2.2 mg/g Cu. Potential acidity of tailings collected below the water table varied from 900 to 1,100 kg/metric ton(t) with an acid neutralization potential of 13–47 kg of H_2SO_4 per ton. Statistical analysis of SEM/EDS data did not show a significant difference in the average amounts of any elements ($\alpha > 0.05$) between upstream and downstream tailings. However, the upstream tailings contain more glauconite and chlorite compared to illite at the downstream location.

Figure 1a shows a topographic map of the watersheds that contributes flow to the tailings pile along with surface water sampling locations. Water flowing through the tailings pile originates as surface runoff, baseflow, and groundwater from four primary tributaries (A, B, C, and D) and rainfall that infiltrates directly through the tailings pile surface and small undifferentiated areas directly adjoining the pile (central area). The mine shaft and multiple mine adits are located in the upstream portion of watershed A, so water released from the mine flows downstream and enters the tailings pile. Where each tributary (A, B, C, and D) enters the pile, small pools or wetlands have formed where water is temporarily stored prior to infiltration into the pile. The infiltrated water migrates through the pile as groundwater, eventually discharging as a series of springs and seeps on the down-gradient embankment face. The bedrock underlying the impoundment is highly metamorphosed, containing alternating layers of muscovite schist and quartz-biotite granitic gneiss. The bedrock permeability is one to two orders of magnitude lower than the tailings,

so most water is believed to flow through the tailings and/or discharge pipe. The site has a humid continental climate with average annual precipitation = 124 cm. Precipitation is fairly uniform throughout the year, varying from 8.3 cm per month in December to 12.4 cm/month in May. The average monthly temperature varies from 0 to 20°C (data from http://www.nc-climate.ncsu.edu for Station: 314496—Jefferson 2 E, NC located 9 km from the pile). Figure 1b is a 1998 color infrared aerial photograph of the pile (NCDOT 2010) and shows the location of six monitoring wells that were installed to characterize seepage through the pile.

In 2008, the USEPA began an Emergency Response removal action to stabilize the Ore Knob tailings dam, including excavation of sediment from a downstream sedimentation basin, construction of a channel to divert storm water around the pile, filling four ponds/wetland around the perimeter of the pile, and regrading the embankment face to reduce the slope and control erosion. In 2009, USEPA placed the site on the National Priorities List for eventual cleanup. The overall objective of this research was to understand how the major physical characteristics of the Ore Knob tailings pile control the transport and reaction of water, oxygen, and pollutants within the pile. This information will be used to identify the most efficient approaches for long-term management of the pile. In this paper, we present results of a detailed physical and hydrologic characterization of the pile and use this information to develop a model of saturated water flow through the pile. In subsequent work, this information will be used to develop quantitative models of pollutant generation and transport within the vadose zone of the pile.

Methods

Six soil borings were advanced by hollow stem auger drilling within the tailings pile for collection of soil samples and installation of monitoring wells (Fig. 1b). The thickness of the oxidized layer and depth to the reduced layer and hardpan were determined by visual observation during monitoring well installation and from standard penetration test results. Hand auger borings were also installed at additional locations to provide information on spatial variations in oxidized layer thickness. Particle size analysis was conducted using a Beckman Coulter LS 13–320 laser particle size analyzer equipped with a Universal Liquid Module.

The hydraulic conductivity of the saturated zone was estimated by conducting falling head slug tests in each of the monitoring wells. The pressure response versus time data from the slug tests were analyzed using Hvorslev's method (Schwartz and Zhang 2002). The infiltration capacity of the tailings pile surface was measured immediately adjoining four monitoring wells using a double-ring infiltrometer. At each location, saturated hydraulic conductivity (K_{sat}) was measured using a compact constant head permeameter (CCHP) (Amoozegar 1989).

Undisturbed samples on unconsolidated material were collected using an Uhland sampler. Blocks of consolidated material from the hardpan layers were excavated, shaped, and sealed in 7.6 cm diameter cylinders with paraffin for analysis. Saturated hydraulic conductivity of each sample was measured using the constant head method (Klute and Dirksen 1986). Moisture retention curves were measured on a pressure plate apparatus while applying suction, and monitoring change in moisture content (Klute 1986). Water

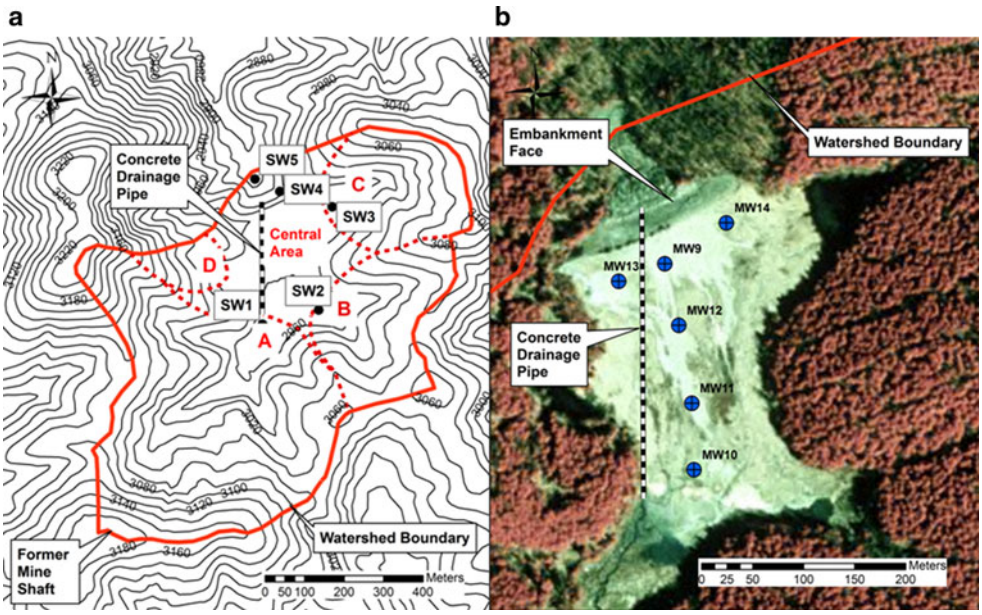

Fig. 1 **a** Topographic map of tailings pile watershed showing four major subwatersheds (*A*, *B*, *C*, and *D*) and surface water monitoring locations. Contours are in feet above mean sea level. **b** Infrared aerial photograph of the tailings pile showing monitor well locations

retention of each material was measured on undisturbed samples at 0–0.4 bar and on disturbed samples at 0.5–15 bar (Klute 1986). The measured pressure—saturation curves were fit to the Brooks and Corey (1964) model using an automated calibration procedure that minimized the root mean square error (RMSE) between simulated and measured water saturation (Patil and Rajput 2009). The effective saturation (S_e) was calculated by:

$$S_e = [(\theta - \theta_r)/(n - \theta_r)] = (\psi/\psi_b)^{\lambda} \quad \text{for } \psi < \psi_b \quad \text{and}$$
$$S_e = 1 \quad \textit{for } \psi \geq \psi_b$$

where θ is the soil water content (V_{water} cm^3/V_{total} cm^3), θ_r is the residual soil water content (V_{water} cm^3/V_{total} cm^3), n is total porosity (V_{void} cm^3/V_{total} cm^3), ψ is capillary pressure of water (cm), ψ_b is bubbling pressure (cm), and λ is pore size distribution index. Saturation-pressure and saturation-permeability curves for soils from the upland watershed were estimated using the Rosetta software (Schaap et al. 2001), based on relationships developed by Van Genuchten (1980) and Mualem (1976) and the particle size distribution (NRCS 2008).

Water samples from monitoring wells were collected using diffusion bag samplers constructed of 2.54 cm (1 inch) diameter regenerated-cellulose dialysis membrane inside an outer protective layer of LDPE mesh. Samplers were installed near the top, middle, and bottom of the saturated zone in each well to monitoring vertical variations in water quality. New dialysis membranes were used during each sampling event and filled deionized water prior to installation. A rubber balloon packer was placed between the top and middle samplers and between the middle and bottom samplers. The balloon packers were intended to reduce mixing in the wells, allowing individual zones to be monitored. However, physically removing the samplers and packers from the wells caused significant mixing and may have limited the effectiveness of this sampling technique in isolating different zones. The samplers were allowed to equilibrate for 1 week.

Surface water was monitored on eight separate dates between March 2007 and August 2008. All samples were collected as grab samples. Whenever possible, samples were collected by fully submerging the sample bottle below the water surface and sealing with no headspace. However, at many of the sampling stations, the water was not deep enough to fully submerge the bottle. The water sample was then transported a few feet to the sampling vehicle where the water samples were passed through a 0.45 μm filter and then placed in individual sample bottles with appropriate preservatives.

The pH, dissolved oxygen (DO), Eh, and temperature were measured in the field immediately after sample collection. DO was measured using colorimetric test kits (CHEMetrics) with a detection limit of 0.1 mg/L; pH, Eh, and temperature were measured using a field meter with a Ag/AgCl reference electrode. Hot acidity (mg/L as $CaCO_3$) was measured by boiling the sample in the presence of hydrogen peroxide and sulfuric acid and then titrating to pH = 8.2 with sodium hydroxide to measure acidity associated with dissolved metals (Clesceri et al. 1989). Samples for metals and sulfate analysis were filtered in the field by pumping through a 0.45 μm disposable cartridge filter. Metals were preserved by acidification to pH < 2 with 2 N nitric acid. No preservative was added to the samples being analyzed for sulfate, which could have allowed a small amount of sulfate to be removed by sorption to precipitated iron oxide residues Dissolved metals were analyzed on a Perkins Elmer Plasma II ion coupled plasma argon emission spectrometer (ICP-AES) following methods equivalent to SW-846 6010C (detection limit = 0.06–0.09 mg/L). Sulfate was analyzed by ion chromatography following methods equivalent to SW-846 9056 (detection limit = 2.5 mg/L). All samples were stored on ice at 4°C for transport to the laboratory. Blank, duplicate, and spiked samples were analyzed during every sampling event.

Tailings Physical and Hydrologic Characteristics

There are significant spatial variations in the physical and hydraulic characteristics of the tailings sediment. Sediments at the up-gradient end of the tailings pile are much finer grained than the material closer to the embankment face. The tailings are believed to have originally been discharged near the embankment, causing more coarse-grained material to settle out near the embankment and finer-grained material to be deposited upstream, near the drop-inlet.

Visual observations indicate the presence of an upper, oxidized zone overlying a deeper reduced zone throughout the tailings pile. The oxidized layer varies in thickness from 0.1 to 0.3 m in the fine-grained sediments near the drop-inlet to 0.8–1 m in the coarse-grained sediment near the embankment face (Fig. 2). Within the oxidized zone, there is a surficial layer of soft, yellow to light brown, fine-grained material that grades into a more densely packed, partially oxidized, dark brown layer. Occasional inclusions of unoxidized material were observed in test pits. Below the oxidized zone, the material transitions to a grey hard-pan layer, which is underlain by loose unconsolidated sediment. Within the reduced layer, there is a gradual transition in color and cementation with depth, from a relatively soft, light grey material to a dark gray, cemented hard pan. Below this hard pan, the vadose zone is much softer and dark blue-gray to black. Standard penetration test blow counts (corrected) vary from 5 to 10 blows per

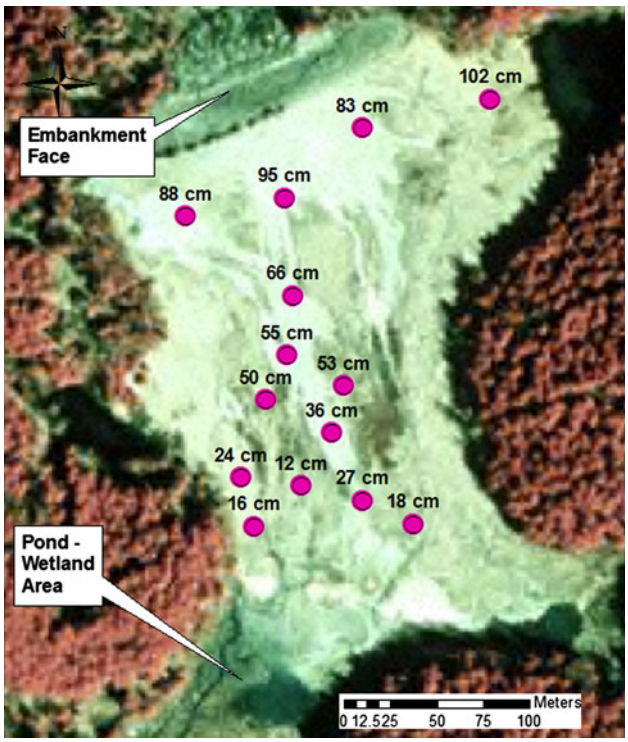

Fig. 2 Depth of oxidized tailings in the Ore Knob tailings pile

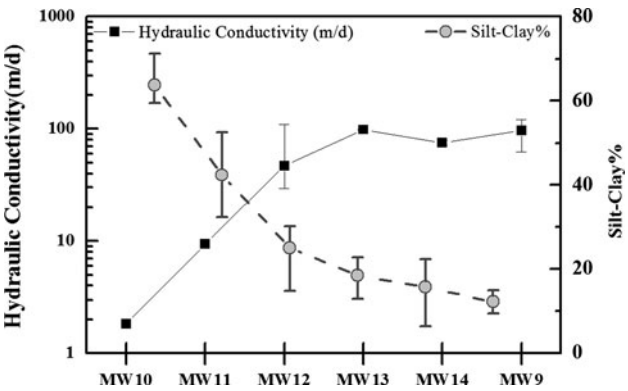

Fig. 3 Silt-clay percent and hydraulic conductivity in different locations at Ore Knob tailings pile (*error bars* are the range of observed values)

foot (bpf) in the oxidized zone to 50–100 bpf in the hardpan, to 5–15 bpf in the reduced coarse-grained sediment. The reduced fine-grain sediment below the hardpan was very soft and would not support the weight of the hammer. The grains of the coarse reduced tailings appear to have been mechanically fractured, with ragged edges and angular shapes. The specific gravity of the reduced tailings varied from 3.2 to 3.6 (ASTM D 854–06).

The hydraulic conductivity of the saturated tailings was determined by conducting rising head slug tests in each monitoring well and analyzing the results following Hvorslev's method (Schwartz and Zhang 2002). Figure 3 shows the spatial variation in hydraulic conductivity and silt–clay content (weight % passing #200 sieve). Hydraulic conductivity increased from MW10 near the drop-inlet to MW9 near the embankment face, consistent with the decline in silt–clay content.

The effective permeability of the vadose zone sediments immediately adjoining four monitoring wells (MW10, MW11, MW12, MW13) were measured using three different techniques: (1) saturated infiltration rate was measured in the field using a double-ring infiltrometer (Bouwer 1986); (2) saturated hydraulic conductivity was measured in the field using a CCHP; and (3) saturated hydraulic conductivity was measured on cores of hardpan material in the laboratory using constant head method (Klute and Dirksen 1986). Results of the vadose zone permeability testing are summarized in Table 1.

The three testing methods generated relatively consistent results. Infiltration rates were highest near the embankment face and declined towards the drop-inlet, consistent with the decline in sediment grain size. Saturated hydraulic conductivity (K_{sat}) values in the yellow–brown layer measured with the CCHP showed much less variability. Both the double ring infiltration and CCHP results indicate a modest decline in permeability from the oxidized to the reduced zone above the hard pan. However, the lab permeameter results indicate an increase in permeability in the hard pan layer. Overall, there is no evidence that oxidation of the tailings or formation of the hardpan resulted in a major change in permeability.

Effect of Weathering on Physical and Hydraulic Characteristics

A more detailed characterization of the surficial sediments was conducted at two locations (MW10 and MW13) to evaluate the impact of weathering on water and oxygen transport. Pressure–saturation curves were measured on undisturbed soil samples obtained at several depths at MW10 and MW13 (Fig. 4). The major physical and hydraulic characteristics of the tailings at each location are summarized in Table 2.

In the upstream location (MW10), sediment characteristics were relatively consistent with depth, indicating that weathering processes have not had a major impact on the physical and hydraulic characteristics of the tailings. Throughout the profile, the sediments are fine grained (D_{50} = 40 to 150 μm), with a relatively constant fine fraction (D_{10} = 3–11 μm) and porosity (0.43–0.48). All of the pressure–saturation curves at MW10 followed the same general pattern (Fig. 4), indicating a consistent pore size distribution.

At the downstream location (MW13), there are significant differences in the physical and hydraulic characteristics with depth. Below 0.5 m, the tailing are relatively coarse

Table 1 Vadose zone permeability results

Method	Field double ring infiltration rate (cm/d)		Saturated hydraulic conductivity (cm/d)			
			Field measurement with CCHP		Constant head lab permeameter	
Layer	Oxidized, yellow–brown	Reduced, gray	Oxidized, yellow–brown	Reduced, gray	Oxidized, yellow–brown	Hard pan, gray
MW13	237	173	79	71	105	197
MW12	153	130	75	31	NA	–
MW11	112	59	82	42	NA	–
MW10	30	27	56	43	NA	49

NA not analyzed

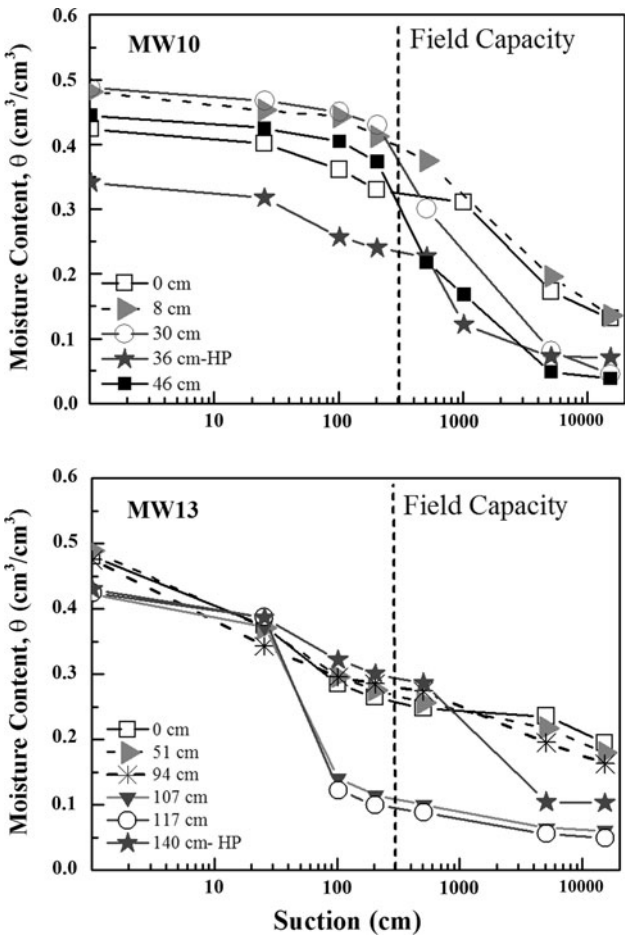

Fig. 4 Water retention capacity for fine grained (MW10) and coarse grained (MW13) tailings in different depth based on visual appearance of the tailings

grained (D_{50} = 239–407 μm). However, from 0 to 0.5 m below the ground surface, weathering has increased the amount of fine-grained material (D_{10} = 1–4 μm), resulting in a broader pore size distribution. This is reflected in the steady decline in moisture content with increasing capillary suction in the MW13 oxidized sediments (Fig. 4). In the less extensively weathered material immediately above the hardpan, there is much less fine grained material (D_{10} = 105–154 μm), resulting in a narrow pore size distribution and abrupt breaks in the pressure–saturation curves (Fig. 4). The hardpan layer contains more fine-grained material (D_{10} = 54 μm), with a pressure–saturation curve that is intermediate between the shallow oxidized tailings and deeper reduced material.

Differences in the physical characteristics of the sediment at MW10 and MW13 are reflected in air-filled porosity and effective oxygen diffusivity at each location. Figure 5 shows profiles of total porosity and moisture content versus depth measured in cores at MW10 and MW13 measured in July 2009 (Table 2). Effective diffusivity of oxygen through the unsaturated tailings was computed using a relationship developed by Reardon and Moddle (1985). Air-filled porosity was computed as the difference between the total porosity and volumetric moisture content. At MW10, the large amount of fine-grained material resulted in a relatively high moisture content (0.32–0.37), low air-filled porosity (0.1–0.13), and low oxygen diffusivity throughout the profile. At MW13, the variations in sediment characteristics with depth resulted in large variations in air-filled porosity and oxygen diffusivity. In the oxidized zone, the larger amount of fine material causes more water to be retained, reducing the air-filled porosity and effective diffusivity. In the reduced zone above the hardpan (1.1–1.2 m), the much lower field capacity of this material allows the water to drain away, resulting in a higher air-filled porosity and effective diffusivity (note difference in diffusivity scale for MW10 and MW13). However, in the hardpan, the increase in fine material causes more water to be retained, reducing the effective oxygen diffusivity. Deeper in the pile, the tailings are saturated, resulting in very low oxygen diffusivity.

Water Flow Through the Tailings Pile

Water flowing through the tailings pile originates as surface runoff and baseflow from four primary tributaries, several small undifferentiated areas, and rainfall that

Table 2 Physical properties of fine-grained (MW10) and coarse-grained (MW13) tailings

		Depth [m]	D_{10} [mm]	D_{50} [mm]	Silt + clay [%]	Porosity (n)	Ambient water content (θ)	Ambient air-filled porosity (Φ)	Irreducible water content (θ_{wr})	Pore size distribution factor (λ)	Bubbling pressure (ψ_b) [cm]
MW10-fine tailings	Ox, y	0	3	91	38	0.44	0.32	0.12	0.13	0.23	24.64
	Ox, br-or	0.08	7.0	78.9	37	0.46	0.33	0.13	0.14	0.19	30.53
	Red, gr	0.30	11	61	48	0.48	0.37	0.11	0.05	0.23	37.82
	Hardpan	0.36	9	153	29	0.46	0.36	0.10	0.07	0.25	20.58
	B har	0.46	4	40	62	0.44	0.32	0.12	0.04	0.23	31.51
	B WT	5.5	6	45	59	0.43	0.43	0.00	NA	NA	NA
	B WT	7	3	30	85	0.45	0.45	0.00	NA	NA	NA
	B WT	10	1.6	12.4	99	0.47	0.47	0.00	NA	NA	NA
MW13-coarse tailings	Ox, y	0	3	90	36	0.46	0.33	0.13	0.19	0.40	7.28
	Ox, br-or	0.34	1	31	64	0.46	0.34	0.12	NA	NA	NA
	Ox, d br	0.51	4	383	30	0.45	0.29	0.16	0.18	0.32	5.39
	Ox, p y	0.94	85	379	8	0.50	0.29	0.21	0.12	0.41	15.00
	Pale gr	1.07	105	316	5	0.48	0.22	0.26	0.06	0.88	21.46
	Red, d gr	1.17	154	350	4	0.46	0.21	0.25	0.05	0.97	22.76
	Hardpan	1.40	54	389	10	0.45	0.25	0.20	0.10	0.23	16.16
	B har	1.73	90	366	8	0.48	0.29	0.19	NA	NA	NA
	B WT	12	78	239	8	0.44	0.44	0.00	NA	NA	NA
	B WT	14	41	407	12	0.46	0.46	0.00	NA	NA	NA
	B WT	16	83	248	8	0.44	0.44	0.00	NA	NA	NA
	B WT	17	114	313	5	0.42	0.42	0.00	NA	NA	NA
	B WT	18	50	257	11	0.44	0.44	0.00	NA	NA	NA

NA not available, *Ox* oxidized, *Red* reduced, *y* yellow, *br* brown, *or* orange, *gr* gray, *d* dark, *p* pale, *B* below, *WT* water table, *har* hardpan

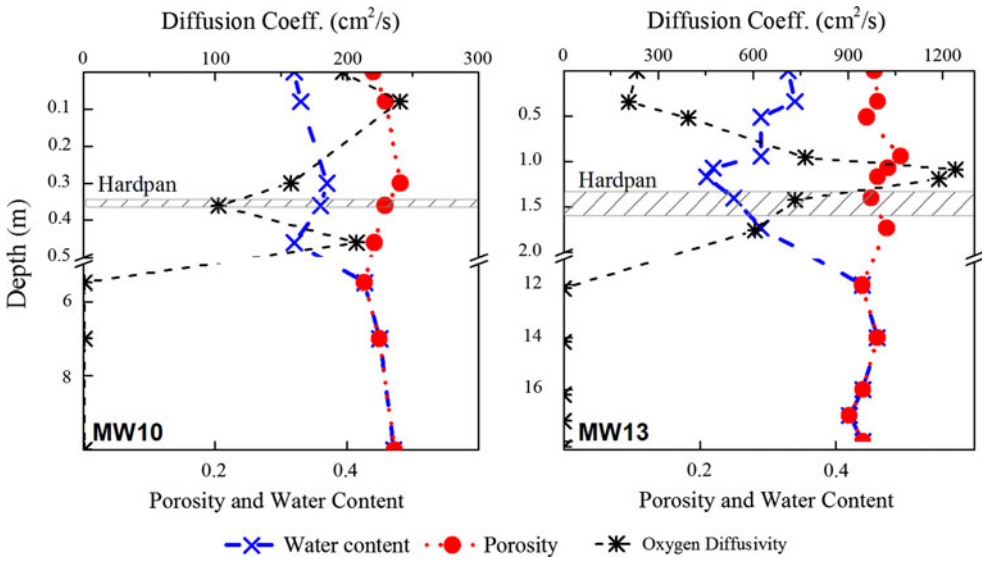

Fig. 5 Variation in total porosity, water content, and effective oxygen diffusivity versus depth in fine grained (MW10) and coarse grained (MW13) tailings

infiltrates directly through the tailings pile surface. Where the primary tributaries enter the pile, the water table rises to the ground surface and small pools or wetlands have formed. Water is temporarily stored in these pools prior to infiltration, then migrates through the pile as saturated flow, eventually discharging as a series of springs and seeps on the down-gradient embankment face. The original concrete drainage pipe is still present within the pile and flow can sometimes be observed entering the drop-inlet. However, the pipe outlet is periodically blocked by

sediment. During some periods, large amounts of water can be observed discharging from a large hole in the embankment face, indicating that the pipe is carrying a substantial flow. However, during other periods, the hole becomes blocked with accumulated sediment and there is no evidence of a concentrated discharge. As a result, the fraction of flow transported as groundwater seepage versus that carried by the pipe varies considerably, with no consistent pattern.

Water table (WT) elevations in each monitoring well were measured monthly from July 2007 to August 2008 by manual monitoring and continuously recording pressure transducers. In general, WT elevations were reasonably constant over the monitoring period. Water level fluctuations were greatest in MW10, closely adjoining the up-gradient pond-wetland. Water levels in MW10 responded relatively rapidly to rainfall events, indicating a good hydraulic connection between the pond and the WT in the tailings pile. For all other wells, water levels were relatively constant and declined gradually due to an extended drought.

Figure 6 shows a profile extending from MW10 through the tailings pile to the embankment face. Water table elevations are average values over the monitoring period. Bedrock and land surface elevations are based on results on from soil borings. In the vast majority of the tailing pile, the WT is deep (2–10 m below ground surface) with no evidence of perched water tables. The hydraulic gradient between MW10 and MW11 is very small, suggesting some water is being transmitted through this area by the concrete drainage pipe. From MW11 to MW9 near the embankment face, the hydraulic gradient is much greater, consistent with more rapid groundwater flow in this area. The WT elevation in MW14 was consistently higher than in MW9 and MW13, indicating a hydraulic gradient from the east to west, possibly due to recharge from tributary C.

Average groundwater flow velocities between well pairs were calculated based on the average hydraulic gradient and average permeability. Calculated groundwater velocities were 0.1 m/d from MW10 to MW11, 3.7 m/d from MW11 to MW12, and 7.9 m/d from MW12 to MW9. The high groundwater velocity from MW11 to MW9 was due to the large amount of water recharging the pile from the tributaries and the high permeability of the tailings. The low velocity calculated between MW10 and MW11 may be due to a significant amount of flow being carried through this zone by the concrete pipe. Alternatively, the actual velocity may be higher than the calculated velocity, if the measured hydraulic conductivity (K) in MW10 (K = 2 m/d) is not representative of this portion of the tailings pile.

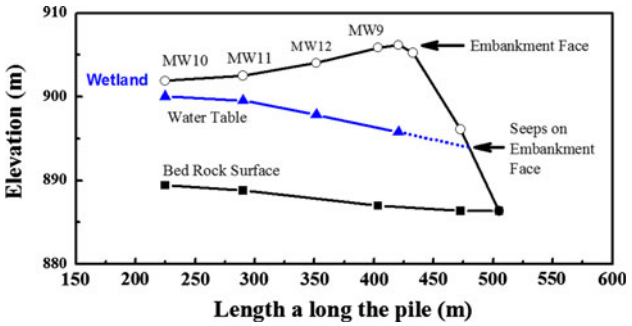

Fig. 6 Average water table profile through the tailings pile

Modeling Recharge and Water Flow Through the Tailings Pile

Efficient management of AMD requires a quantitative understanding of water movement through the tailings pile. In this section, surface recharge and stream flow entering the pile were estimated and used to calibrate a groundwater flow model and evaluate the effect of different management strategies on water table position.

Surface runoff and recharge were estimated for the period from when the mine closed in 1960 to 2009, using the water balance model DRAINMOD (Skaggs 1982; Skaggs and Tabrizi 1981), which performs a continuous water balance in the soil profile. DRAINMOD was used to simulate daily evapotranspiration (ET), surface runoff, and deep recharge for three different areas: (1) coarse-grained tailings near MW13, (2) fine-grained tailings near MW10, and (3) watershed soils contributing stream flow to the pile. Model input included meterological data, pressure saturation curves, and hydraulic conductivity at varying depths (Skaggs and Tabrizi 1981). The hydraulic characteristics of the watershed soil were estimated from the particle size distribution (NRCS (Natural Resources Conservation Service) 2008), following procedures described by Saxton et al. (1986). Daily rainfall, temperature, and evapotranspiration were estimated from monitoring data collected at site ID#314496—Jefferson 2 E, located 9 km away at 844 m above sea level (State Climate Office of North Carolina 2010).

Figure 7 shows estimated annual ET, recharge, and surface runoff from the coarse-grained (MW13), fine-grained (MW10), and watershed areas for driest year, wettest year, and long-term average for the period from 1960 to 2009. Runoff was generally not a major fraction of the overall water budget. ET was highest in the up-gradient watershed due to the extensive vegetative cover. Near MW13, the coarse-grained tailings allowed rapid recharge, reducing ET and runoff. The relatively high average annual recharge into the tailings, 64–86 cm/year, rapidly transports acidity produced within the vadose zone to the water table surface.

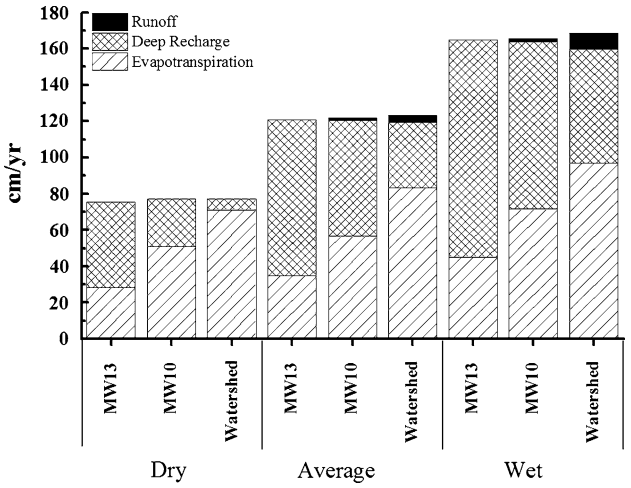

Fig. 7 Variation in runoff, evapotranspiration, deep recharge in coarse grained (MW13), fine grained (MW10) and watershed areas for driest, average and wettest years

Saturated flow through the tailings pile was simulated using MODFLOW (Harbaugh et al. 2000). The tailings pile was represented as a seven layer grid. The permeability distribution was estimated from slug tests on the monitoring wells (Fig. 3). The transition from tailings to bedrock was estimated from the observed bedrock elevations and surrounding topography. Seeps along the embankment face were represented as drains. Recharge rates into the tailings surface were estimated from the calculated infiltration. All runoff and baseflow from tributaries B, C, and D entered the pile as recharge from the ponds/wetlands at each location.

During the initial model testing, it was apparent that MODFLOW could not be accurately calibrated to match the observed water levels in the pile due to the low permeability of the tailings in the upstream area. The simulated water table (WT) elevations at the upstream end of the pile were much too high and the WT was too low in the middle and downstream ends of the pile. Two potential alternatives were identified to explain the error in model calibration and were evaluated using MODFLOW. Under Alternative A, the hydraulic conductivity (K) in the upstream area was assumed to be 20 times higher than the value measured in MW10. Alternative A provided an adequate match to the observed WT data (mean calibration error = 0.20 m, root mean squared error (RMSE) = 0.86 m). However, the very high K value used in the simulation is not reasonable in light of the fine-grained material present throughout the area. Under Alternative B, a portion of the flow was assumed to be carried from the upstream area to the middle of the pile by the concrete pipe and/or natural soil beneath the pile. This effect was represented in the model by a single row of high permeability cells. Figure 8 shows simulated water table elevations in the tailings pile under the Alternative B

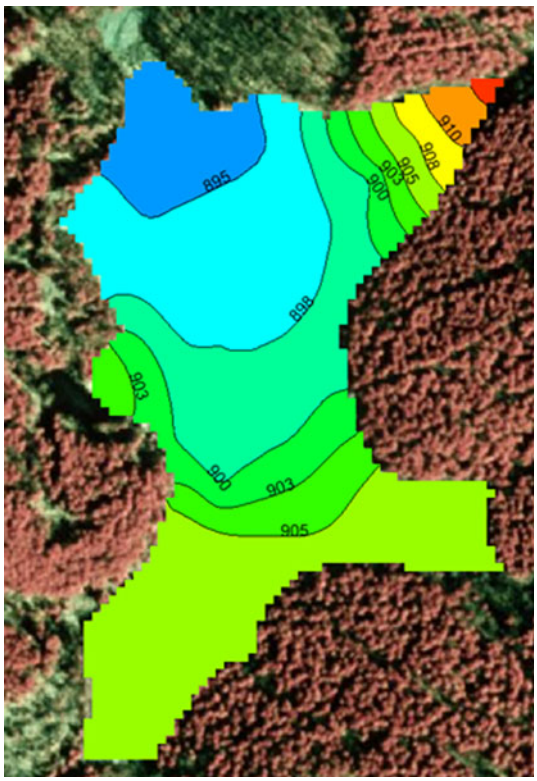

Fig. 8 Simulated water table elevations in tailings pile for Alternative B. Contour interval is meters above mean sea level

assumptions. Overall, Alternative B provided a slightly better fit to the observed WT data (mean error = −0.08 m, RMSE = 0.66 m) and accurately matched the locations where water ponds above the tailings surface. Most water enters the pile from these ponds and discharges as seeps along the embankment face. More importantly, Alternative B is much more reasonable given the flow observed to enter the concrete pipe, but not to discharge from the pipe. Unfortunately, there is no way to directly verify the validity of Alternative B.

As part of the emergency response action, USEPA will plug the concrete drainage pipe and excavate an emergency bypass channel/spillway to carry storm water from tributary A around the eastern edge of the pile, crossing tributaries B and C, and ultimately discharging into Ore Knob Branch downstream of the pile. The effect of plugging the concrete pipe and construction of the bypass channel was simulated using MODFLOW by representing the channel as a drain (Fig. 9). Under existing conditions, the vadose zone thickness is zero (WT is above the tailings surface) for 44% of the pile, 0–2 m thick for 7% of the pile, and over 2 m thick for 49% of the pile. After plugging the concrete pipe and completion of the bypass channel, seepage at the embankment face should be reduced by about 58%, and the portion of the pile saturated to the land surface should be reduced by 0.6 ha to 37% of the pile

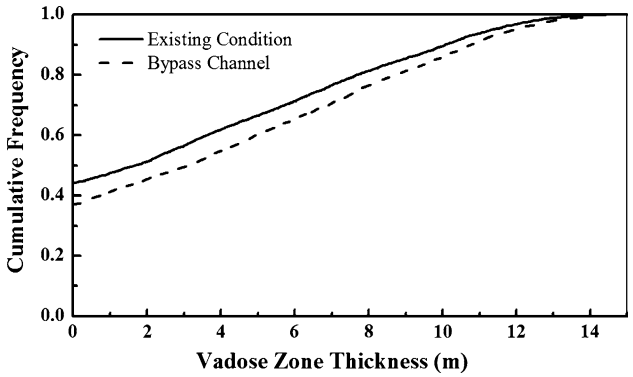

Fig. 9 Cumulative frequency distribution for vadose zone thickness under existing conditions (Alternative B) and after plugging the concrete pipe and construction of the bypass channel

surface. However, the bypass channel is expected to have minimal impact on the water table elevations near the embankment face. Diverting flow around the pile may slow the transport of acidity out of the pile. However, the increase in unsaturated tailings could potentially increase overall acidity production by allowing greater oxygen penetration into the pile.

Subsurface and Surface Water Quality

Ground Water

Six fully screened groundwater monitoring wells were sampled on five separate occasions in 2007–2008 to monitoring temporal and spatial variations in geochemical parameters. Average values for each of the monitored groundwater parameters are presented in Table S-1 (supplementary material). Bromide (Br), nitrite (NO_2), nitrate (NO_3), and phosphate (PO_4) were below detection in all samples and are not shown in Table S-1. The field Eh measurements are corrected to a standard hydrogen electrode so the values are approximately 240 mV higher than are commonly reported for 'uncorrected' electrodes. DO was measured in the field using disposable Chemetrics ampoules. Measured hot acidity values closely matched theoretical values (1–6% difference) estimated using a relationship developed by Kirby and Cravotta (2005), which accounts for acidity associated with Fe(II), Fe(III), Mn, Al, and free protons (H^+).

As groundwater migrates down-gradient through the tailings, dissolved iron, sulfate, and acidity increase dramatically. During migration from MW10 to MW9, SO_4 increases by 967 mg/L as S and Fe increases by 1,786 mg/L, a ratio of 1.20 mol of SO_4 per mole Fe, consistent with the oxidation of pyrrhotite. SO_4 concentrations measured by ion chromatography are very similar to total S concentrations measured by ICP-AES, indicating that essentially all of the dissolved S is present as SO_4, with insignificant levels of other sulfur species. In the down-gradient wells (MW13, MW9, and MW14), pH values are moderate (5.8–6.1), even though the groundwater contains extremely high levels of hot acidity. In samples with high acidity levels (>500 mg/L), more than 98% of the acidity was typically associated with Fe^{2+}. Free protons (H^+) are not released until Fe^{+2} reacts with oxygen, when the AMD is discharged at the land surface.

Groundwater samples were collected and analyzed for aluminum (Al), arsenic (As), cadmium (Cd), cobalt (Co), chromium (Cr), copper (Cu), nickel (Ni), lead (Pb), and zinc (Zn). As, Cd, Co, Cr, Ni, and Pb were below analytical detection limits in all samples (0.06–0.09 mg/L). Zn concentrations increased from up-gradient to down-gradient wells, following the same general trend as SO_4. Cu concentrations were relatively low all samples, varying between 0.06 and 0.11 mg/L. Average Al concentrations were below 0.2 mg/L in MW10, MW11, MW12, and MW14 and below 1.0 mg/L in MW13 and MW9. The slightly elevated aluminum values in MW13 and MW9 are likely associated with the slightly lower pH in these wells, which increased the effective solubility of Al. Ca was the cation present at the highest concentration (excluding Fe), followed by Mg, K, and Na. Silica (Si) concentrations were lowest in the up-gradient wells (5–10 mg/L), gradually increasing to 30–40 mg/L in the down-gradient wells.

In every well, there was a consistent trend of declining Eh and DO with depth, indicating more reducing, anaerobic conditions at increased depth below the WT. DO values were highest in the most up-gradient well, possibly due to influx of oxygenated water from the up-gradient pond-wetland. In all of the down-gradient wells, pH was lowest, and Fe, SO_4, and acidity were highest in the top sample interval. This is consistent with recharge of concentrated AMD through the vadose zone. Since some mixing probably occurs in the monitoring wells, the observed differences between the top, middle, and bottom samples are probably the minimum that actually occurs within the pile.

Surface Water

Surface water was periodically monitored at four locations surrounding the tailings pile (SW1, SW2, SW3, SW4, and SW5) and at two downstream locations (SW6 and SW7). SW1 is located at the large pond-wetland at the upstream end of the tailings pile. There are several mine adits in the upper portion of the SW1 watershed, some of which were treated with anoxic limestone drains in the 1980s. Analytical results for SW-2 were similar to SW-3. However, SW-2 was sampled much less frequently and will not be discussed further. SW3 is located at a small pond on the

eastern edge of the tailings pile near the embankment face. There are no known mine discharges in the SW3 watershed. SW4 monitors a large seep on the eastern edge of the embankment face and is believed to be representative of concentrated acid seeps discharging from the tailings pile. SW5 is located on Ore Knob Branch, a short distance downstream from the pile, and includes all seepage from the tailings pile and water that may have passed through the concrete drainage pipe in the tailings pile. SW6 is located on Ore Knob Branch, 1.2 km downstream from the tailings pile and immediately upstream of the confluence with Peak Creek. SW7 is located on Peak Creek a short distance upstream of where it joins with Ore Knob Branch and is representative of background water quality.

All of these surface water monitoring locations were sampled on eight separate dates between March 2007 and August 2008. Average values and standard deviations for each of the parameters are presented in Table S-2. The pH was well below the surface water quality standard of 6 in all sampling stations within the Ore Knob Branch watershed. The only station that met the pH standard was SW8, which is a background station not impacted by the mine. Dissolved iron, sulfate, and hot acidity concentrations discharging from the tailings pile (SW4 and SW5) are much higher than water entering the pile, indicating that most acidity is produced within the pile. Average dissolved iron concentrations in SW1 were 62 mg/L, compared to 11–12 mg/L in well MW10, which is located a short distance down-gradient within the tailings pile. The substantial decline in dissolved iron from SW1 to MW10 suggests that some dissolved iron is being removed as water infiltrates into the tailings pile. In contrast, sulfate increased dramatically from 275 mg/L in SW1 to 1,700–1,900 mg/L in MW10. The cause of this dramatic increase is not understood. Dissolved iron and sulfate levels in SW1 are significantly higher than in SW3, indicating that the upstream mine and adits do contribute substantial amounts of AMD.

Surface water discharging from the tailings pile (SW4 and SW5) contains extremely high concentrations of Fe, SO_4, and acidity. As this water migrates downstream along Ore Knob Branch to SW7, the pH decreases to 3.1, due to oxidation of Fe^{+2} and the formation of $Fe(OH)_3$ and H^+. At the point where Ore Knob Branch discharges into Peak Creek (SW6), the stream still carries 285 mg/L of acidity (as $CaCO_3$).

Surface water samples were collected and analyzed for Al, As, Cd, Co, Cr, Cu, Ni, Pb, and Zn. Arsenic, Cd, Co, Cr, Ni, and Pb were below the analytical detection limit in all samples, and will not be discussed further. Average Cu concentrations entering the tailings pile from the upstream watershed were very high (1–2 orders of magnitude above the NC surface water standard). Cu concentrations discharging from the tailings pile were lower, but still over 40 times the surface water standard. There was only a small decline in Cu during transport downstream through Ore Knob Branch, indicating little Cu attenuation other than dilution. Zn concentrations entering the pile were high and increased due to AMD production within the pile.

Pollutant Budgets

An overall pollutant budget was developed for the tailings pile to evaluate the relative contributions of water and pollutants entering from the upstream mine impacted areas (watershed A on Fig. 1), un-impacted areas (watersheds B, C, and D on Fig. 1), and infiltration through the tailings pile surface. Average flow rates from each of these areas were calculated using the runoff, ET, and recharge estimates generated by DRAINMOD. Pollutant loads in surface water were calculated as the average flow rate for each watershed times the average pollutant concentration. Watershed C, which contains SW-3, does not contain any mine related features and was assumed to be representative of other watersheds (B and D) that do not contain mine adits or spoil piles. The pollutant load generated by

Table 3 Average dissolved pollutant budget for Ore Knob Mine tailings pile

	Average concentration in surface water entering pile (mg/L)			Total pollutant load (kg/year)		
	Mine impacted (SW-1)	Unimpacted (SW-3)	Combined discharge (SW-5)	Upstream watershed	Recharge through pile surface	Combined discharge
Flow (m^3/d)	580	510	1,300			
Acidity	170	110	930	26,000	220,000	250,000
Fe	62	12	410	7,500	100,000	110,000
SO_4	280	140	1,500	40,000	370,000	410,000
Mn	1.2	0.2	3.9	140	900	1,000
Al	1.0	2.1	9.8	260	2,400	2,600
Cu	0.5	0.3	0.3	80	−5	75
Zn	0.7	0.2	1.4	87	280	370

recharge through the tailings pile surface was calculated as the difference between the surface water load entering the pile from the upstream watershed and the combined load discharging to Ore Knob Branch.

Results of the pollutant budget analysis are presented in Table 3. Recharge through the tailings pile surface contributes 14% of the total discharge, but carries most of the pollutants. Watershed A, which contains the mine adits, releases 26 t/year of acidity, while 221 t/year of acidity are generated by oxidation within the tailings pile. The only exception to this overall trend is copper, where the calculated load discharging from the pile was essentially the same as the load entering the pile in the surface water, indicating that little or no copper was released from the tailings. This is consistent with the low copper concentrations measured in the monitoring wells in the pile.

Discussion and Conclusions

A pollutant budget analysis indicates that over 89% of the dissolved iron, sulfate, aluminum, and acidity released to Ore Knob Branch are produced in the vadose zone of the pile. These AMD constituents are rapidly transported through the pile by surface water from the upstream watershed. Given the tremendous mass of acidity produced within the pile (approximately 220 t/year), long-term treatment of the discharge is not practical.

Significant spatial variations in the physical and hydraulic characteristics of the tailings cause large variations in air-filled porosity and effective oxygen diffusion in the tailings pile. Tailings in the upstream areas are finer grained, with less air-filled porosity and oxygen diffusivity. The original tailings in the downstream areas are coarser grained, with lower water retention and higher oxygen diffusivity. However, weathering processes have increased the fine-grained fraction in the oxidized zone and hardpan layer, increasing water retention and decreasing oxygen diffusivity. The thickness of the downstream oxidized zone combined with this increased water retention may have significantly reduced acidity generation in the downstream areas.

Due to concerns over the stability of the tailings pile slope and potential overtopping of the embankment during flood events, the USEPA is regrading the embankment face and constructing a diversion channel around the tailings pile. These changes are expected to substantially reduce water flow through the pile, reducing the vector that transports AMD into Ore Knob Branch. However, these modifications will also lower the water table in upstream portions of the pile where acidity production is now relatively low. It is not clear whether lowering the water table in the upstream areas will significantly increase acid production since the tailings in this area are fine grained and retain substantial water even when the water table is low. A quantitative model capable of simulating saturated–unsaturated flow, oxygen transport, and geochemical reactions is required to address this issue.

Acknowledgments We thank the North Carolina Dept of Environmental Management and U.S. Environmental Protection Agency for the financial and technical support they provided for this project.

References

Amoozegar A (1989) A compact constant head permeameter for measuring saturated hydraulic conductivity of the vadose zone. Soil Sci Soc Am J 53:1356–1361

Behrooz M (2012) Acid mine drainage production from the Ore Knob tailings pile-characterization and hydrogeochemical modeling. Ph.D. dissertation, Department of Civil, Construction and Environmental Engineering, North Carolina State University, Raleigh, NC, USA (in preparation)

Blowes DW, Reardon EJ, Cherry JA, Jambor JL (1991) The formation and potential importance of cemented layers in inactive sulfide mine tailings. Geochim Cosmochim Acta 55:965–978. doi:10.1016/0016-7037(91)90155-X

Boorman RS, Watson DM (1976) Chemical processes in abandoned sulphide tailings dumps and environmental implications for northeastern New Brunswick. CIM Bull 69:86–96

Bouwer H (1986) Intake rate: cylinder infiltrometer.In: Method of soil analysis, part 1: physical and mineralogical methods, Chap. 32, 2nd edn. American Society of Agronomy, Soil Science Society of America, Madison, pp 825–844

Brooks RH, Corey AT (1964) Hydraulic properties of porous media. T ASAE 7(1):26–28

Clesceri LS, Greenberg AE, Trussell RR (1989) Acidity-hot peroxide treatment. Standard methods for the examination of water and wastewater, 17th edn. American Public Health Association, Washington, DC, pp 2–33

Escobar B, Buccicardi S, Morales G, Wiertz J (2009) Bacterial oxidation of ferrous iron and RISCs at low temperatures: their effect on acid mine drainage and bioleaching of sulphide minerals. Adv Mater Res 71–73:433–436

Evangelou VP, Zhang YL (1995) A review: pyrite oxidation mechanisms and acid mine drainage prevention. Crit Rev Environ Sci Technol 25:141–199. doi:10.1080/10643389509388477

Fennemore G, Chadneller W, Davis A (1998) Modeling pyrite oxidation in arid environments. Environ Sci Technol 32:2680–2687. doi:10.1021/es970900o

Gilbert SE, Cooke DR, Hollings P (2003) The effects of hardpan layers on the water chemistry from the leaching of pyrrhotite tailings material. Environ Geol 44:687–697. doi:10.1007/s00254-003-0810-5

Gunsinger MR, Ptacek CJ, Blowes DW, Jambor JL (2006) Evaluation of long-term sulfide oxidation processes within pyrrhotite-rich tailings, Lynn Lake, Manitoba. J Contam Hydrol 83:149–170

Harbaugh AW, Banta ER, Hill MC, McDonald MG (2000) MODFLOW-2000, The US geological survey modular ground-water model: user guide to modularization concepts and the ground-water flow process. USGS OFR 00–92, Washington, DC

Jaynes DB, Rogowski AS, Pionke HB (1984) Acid mine drainage from reclaimed coal strip mines: 1. model description. Water Resour Res 20:233–242. doi:10.1029/WR020i002p00233

Johnson RH, Blowes DW, Robertson WD, Jambor JL (2000) The hydrogeochemistry of the Nickel Rim mine tailings impoundment, Sudbury, Ontario. J Contam Hydrol 41(1–2):49–80. doi:10.1016/S0169-7722(99)00068-6

Kinkel Jr AR (1967) The Ore Knob copper deposit North Carolina, and other massive sulfide deposits of the Appalachians. USGS Profess Paper 558, Washington DC

Kirby CS, Cravotta CA III (2005) Net alkalinity and net acidity 2: practical considerations. Appl Geochem 20:1941–1964

Klute A (1986) Water retention: laboratory methods. In: Method of soil analysis; part 1: physical and mineralogical methods, Chap. 26, 2nd edn. American Society of Agronomy, Soil Science Society of America, Madison, pp 635–660

Klute A, Dirksen C (1986) Hydraulic conductivity and diffusivity: laboratory methods. In: Method of soil analysis; part 1: physical and mineralogical methods, Chap. 28, 2nd edn. American Society of Agronomy, Soil Science Society of America, Madison, pp 687–732

Lottermoser B (2007) Mine wastes: characteristics, treatment, environmental impacts, 2nd edn. Springer, Berlin, pp 37–38

McGregor RG, Blowes DW, Jambor JL, Robertson WL (1998) The solid-phase controls on the mobility of heavy metals at the Copper Cliff tailings area. Sudbury, Ontario, Canada. J Contam Hydrol 33:247–271. doi:10.1016/S0169-7722(98)00060-6

McSweeney K, Madison FW (1988) Formation of a cemented subsurface horizon in sulfidic mine waste. J Environ Qual 17(2):256–262. doi:10.1016/0016-7037(91)90155-X

Mualem Y (1976) A new model for predicting the hydraulic conductivity of unsaturated porous media. Water Resour Res 12:513–522

NCDOT (North Carolina Dept of Transportation) (2010) GIS (1998) Color-infrared digital ortho mosaics. http://www.ncdot.org/it/gis/DataDistribution/1998colIR/default.html

Nicholson RV, Gillham RW, Cherry JA, Reardon EJ (1989) Reduction of acid generation in mine tailings through the use of moisture-retaining cover layers as oxygen barriers. Can Geotech J 26:1–8

Nordstrom DK, Alpers CN (1999) Geochemistry of acid mine waters. In: Plumlee GS, Logson MJ (Eds), The environmental geochemistry of mineral deposits, Rev Econ Geol 6A:133–160

NRCS (Natural Resources Conservation Service) (2008) Uploaded soil survey data for Ore Knob tailings pile and watershed, version 8, Jan 15 2008. http://websoilsurvey.nrcs.usda.gov/app/WebSoilSurvey.aspx

Pantelis G, Ritchie AIM (1991) Macroscopic transport mechanisms as rate-limiting factor in dump leaching of pyritic ores. Appl Math Model 15:136–143. doi:10.1016/0307-904X(92)90005-N

Parker G, Robertson A (1999) Acid Drainage. The Australian Mineral and Energy Environment Foundation, Sydney. Occasional Paper No 11, pp 101–117

Patil NG, Rajput GS (2009) Evaluation of water retention functions and computer program "Rosetta" in predicting soil water characteristics of seasonally impounded shrink-swell soils. J Irrig Drain E-ASCE 135(3):286–294

Plumlee GS (1999) The environmental geology of mineral deposits. In: Plumlee GS, Logsdon MS (Eds) The environmental geochemistry of mineral deposits, part a: processes, techniques and health issues, Society of Economic Geologists, Littleton. Rev Econ Geol 6A: 71–116

Rankin HS, Stuckey JL (1943) Copper deposits of Western North Carolina. TVA and NC Div Mineral Resources, Knoxville

Reardon EJ, Moddle PM (1985) Gas diffusion coefficient measurements on uranium mill tailings: implications to cover design. Uranium 2:111–131

Rose AW, Cravotta CA III (1998) Geochemistry of coal mine drainage. Coal mine drainage prediction and pollution prevention in Pennsylvania, Chap. 1, PA Department of Environmental Protection, Harrisburg, http://www.dep.state.pa.us/dep/deputate/miners/districts/cmdp/chap01.html

Saxton KE, Rawls WJ, Romberger JS, Papendick RI (1986) Estimating generalized soil-water characteristics from texture. Soil Sci Soc Am J 50(4):1031–1036

Schaap MG, Leij FJ, Van Genuchten MTh (2001) Rosetta: a computer program for estimating soil hydraulic parameters with hierarchical pedotransfer functions. J Hydrol 251(3–4):163–176

Schmiermund RL (2000) Non-acidic, sulfate poor, copper-enriched drainage from a Precambrian stratabound chalcopyrite/pyrite deposit, Carbon County, Wyoming. In: Proceedings, 5th international conference on acid rock drainage, vol 2, Soc for mining, metallurgy, and exploration, Littleton, p 1059–1070

Schwartz FW, Zhang Hubao (2002) Fundamentals of ground water. Wiley, New York City, pp 273–277

Singer PC, Stumm W (1970) Acidic mine drainage: the rate-determining step. Science 167:1121–1123. doi:10.1126/science.167.3921.1121

Skaggs RW (1982) Field evaluation of water management simulation model. T ASAE 25(3):666–674

Skaggs RW, Tabrizi AN (1981) Effect of drainage system design and soil properties on runoff from artificially drained lands. USDA Agricultural Research (Southern Region), New Orleans, pp 311–312

State Climate Office of North Carolina (2010) Uploaded data for 1960–2010. http://www.nc-climate.ncsu.edu

Tasse N, Germain D, Dufour C, Tremblay R (1997) Hard-pan formation in the Canadian Malartic mine tailings: implications for the reclamation of the abandoned impoundment. In: Proceedings, 4th international conference of acid rock drainage, vol 4, CANMET, Ottawa, p 1797—1812

USEPA (US Environmental Protection Agency) (2004) Nationwide Identification of hardrock mining sites. USEPA Report 2004-P-00005, OIG, Washington DC

Van Genuchten MTh (1980) A closed-form equation for predicting the hydraulic conductivity of unsaturated soils. Soil Sci Soc Am J 44:892–898. doi:10.2136/sssaj1980.03615995004400050002x

Weast RC (1976) CRC handbook of chemistry and physics, 57th edn. CRC Press, Cleveland, pp 1976–1977

Yanful EK, Bell AV, Woyshner MR (1993) Design of a composite soil cover for an experimental waste rock pile near Newcastle, New Brunswick, Canada. Can Geotech J 30:578–587. doi:10.1139/t93-050